International Communications in Heat and Mass Transfer 129 (2021) 105685

Contents lists available at ScienceDirect

International Communications in Heat and Mass Transfer

journal homepage: www.elsevier.com/locate/ichmt

# Minichannel and minigap classification criteria based on the aspect ratio of the minigeometry: A numerical study

Paweł Dąbrowski [a,*], Ritunesh Kumar [b]

[a] Gdańsk University of Technology, Faculty of Mechanical Engineering and Ship Technology, Institute of Energy, Gdańsk, Poland
[b] Indian Institute of Technology, Department of Mechanical Engineering, Indore, India

ARTICLE INFO

*Keywords:*
Computational fluid dynamics
Gap
Channel
Velocity profile
Power-law
Correlation

ABSTRACT

A detailed numerical investigation has been carried out to analyze the diabatic flow distribution and velocity profile in 18 minigeometries with various aspect ratios for V-type and I-type flow configurations (for 36 cases) assuming ethanol as a working fluid. The aim of the study is to distinguish the value of the aspect ratio for which the flow in minigeometry starts to be two-dimensional (minigap). Cases with a constant Reynolds number of 4167 (variable mass flow rate) were compared. The normalized velocity profiles over the normalized width of the minigeometry acquired from the simulation have been compared with the theoretically calculated profiles based on the one-seventh power-law and turbulent flow theory. The results show that the one-seventh power-law velocity profiles are not consistent with the profiles simulated at an aspect ratio greater than 7. A new correlation for normalized velocity profile incorporating aspect ratio of the minigeometry for minigaps has been proposed. The conclusions are independent of the geometry depth, working fluid, and flow configuration.

## 1. Introduction

An issue that needs to be sorted out while dealing with minigeometries is the definition of a minigap and identifying the features that distinguish the minigap and the minichannel. The classification of channel and gap is critical in the vocabulary of mini/micro geometries, as it has significant importance on the thermohydraulic behavior of the heat sink. Few studies tried to define minigap arbitrarily [1,2]. Zhang et al. [1] emphasize that a minigap is a geometry in which the ratio of width to depth (aspect ratio) is much greater than 1. It seems to be a reasonably intuitive approach but the actual threshold value needs to be determined. Wan and Joshi [2] defined the value of the width to depth ratio as greater than 10 as a minigap. As the channel width to depth ratio crosses a threshold, the influence of the sidewalls on the fluid flow decreases, while the top and bottom walls increases due to the reduced depth of the geometry or the increased width of the geometry. However, the above authors did not perform any calculations or tests to determine the borderline value of the transition between minigeometries. The value of 10 appears to has been chosen arbitrarily. However, the question arises as to a specific cutoff value for minichannel to minigap transition. This study is an attempt to distinguish between minigap and minichannel. To do so, the authors analyzed selected works dealing with minichannels and minigaps to determine the aspect ratio (α) to find the trend regarding the nomenclature of minigeometry. Details of this analysis are presented in Table 1.

After analyzing Table 1, it can be noticed that most of the examined minichannels have a width to depth ratio of about 1, but there are also channels with the above-mentioned ratio even higher than 15. The smallest value of the width to depth ratio, for which the authors of the study called the minigeometry as minigap, is 8.7 [12]. However, there are works where, despite the width to depth ratio even higher than 10, the minigeometries were called minichannels [14–16,20]. The minichannel terminology with the highest width to depth ratio was used by Piasecka [20], the value was 40 in their study.

It can be seen that it is difficult to state unequivocally the transition limit between the minichannel and minigap. It should also be emphasized that the cited works did not focus on the influence of the sidewalls and the upper and lower walls of a given minigeometry on the fluid flow inside it. Also, the decision on whether the investigated geometry is a minigap or a minichannel was often determined arbitrarily. A systematic study taking into account the physical phenomena occurring in minigeometry with width-to-depth ratio changing would be a valuable addition for the advancement of the scientific field.

Alam et al. [25] conducted experimental studies on the flow boiling in a minigap heat exchanger with a width and length of 12.7 mm for ten

* Corresponding author.
*E-mail address:* pawel.dabrowski@pg.edu.pl (P. Dąbrowski).

https://doi.org/10.1016/j.icheatmasstransfer.2021.105685

Available online 22 October 2021

**Nomenclature**

| | |
|---|---|
| $A$ | Cross-section area, $m^2$ |
| $d$ | Depth, m |
| $D_h$ | Hydraulic diameter, m |
| f | Friction factor |
| G | Mass flux, kg/($m^2$·s) |
| $\dot{m}$ | Mass flow rate, kg/s |
| $n$ | Number of points, |
| $p$ | Pressure, Pa |
| $Re$ | Reynolds number |
| $V$ | Velocity, m/s |
| W | Width, m |

*Greek symbols*

| | |
|---|---|
| $\alpha$ | Aspect ratio |
| $\mu$ | Dynamic viscosity, Pa·s |
| $\rho$ | Density, kg/$m^3$ |
| $\sigma$ | Normalized velocity deviation, % |

*Subscripts*

| | |
|---|---|
| $i$ | i-th point |
| $m$ | Mean |
| max | Maximum |
| $n$ | Normalized |
| $t$ | Theoretical calculation |
| $s$ | Simulation |

*Abbreviations*

| | |
|---|---|
| FVM | Finite volume method |
| SST | Shear stress transport |

**Table 1**
Analysis of works on minigeometries in terms of nomenclature depending on the aspect ratio of the minigeometries.

| Authors | W [mm] × d [mm] | $D_h$ [μm] | α | Minigeometry |
|---|---|---|---|---|
| Anbumeenakshi and Thansekhar [3] | 0.42 × 4.2 | 764 | 0.1 | Minichannel |
| Kumar and Singh [4] | 1 × 3 | 1500 | 0.3 | Minichannel |
| Song et al. [5] | 2 × 6 | 3000 | 0.3 | Minichannel |
| Alam et al. [6] | 0.208 × 0.385 | 270 | 0.5 | Minichannel |
| Matthew et al. [7] | 0.3 × 0.6 | 400 | 0.5 | Minichannel |
| Dalkılıç et al. [8] | 0.382 × 0.470 | 421 | 0.8 | Minichannel |
| Krishnan et al. [9] | 0.35 × 0.29 | 317 | 1.2 | Minichannel |
| Wajs et al. [10] | 1 × 0.7 | 824 | 1.4 | Minichannel |
| Şimşek et al. [11] | 0.20 × 0.05 | 80 | 4.0 | Minichannel |
| Hempijid and Kittichaikarn [12] | 13 × 1.5 | 2690 | 8.7 | Minigap |
| Strąk et al. [13] | 16 × 1.7 | 3073 | 9.4 | Minichannel |
| Piasecka et al. [14] | 24 × 1.7 | 3175 | 14.1 | Minichannel |
| Ozer et al. [15] | 23 × 1.5 | 2816 | 15.3 | Minichannel |
| Maciejewska and Piasecka [16] | 26.5 × 1.7 | 3195 | 15.6 | Minichannel |
| Nasr et al. [17] | 0.20 × 0.01 | 19 | 20.0 | Minigap |
| Kabov et al. [18] | 40 × 2 | 3810 | 20.0 | Minigap |
| Xu and Wu [19] | 2.4 × 0.11 | 210 | 21.8 | Minigap |
| Piasecka [20] | 40 × 1 | 1951 | 40.0 | Minichannel |
| Matthew et al. [7] | 25 × 0.6 | 1172 | 41.7 | Minigap |
| Lorenzini et al. [21] | 10 × 0.2 | 392 | 50.0 | Minigap |
| Asrar et al. [22] | 10 × 0.2 | 392 | 50.0 | Minigap |
| Wan and Joshi [2] | 20 × 0.4 | 784 | 50.0 | Minigap |
| Alam et al. [6] | 12.7 × 0.19 | 374 | 66.8 | Minigap |
| Krishnan et al. [23] | 20 × 0.22 | 435 | 90.9 | Minigap |
| Zhang et al. [1] | 10 × 0.1 | 198 | 100.0 | Minigap |
| Bar-Cohen et al. [24] | 20 × 0.184 | 365 | 108.7 | Minigap |

different minigap depths (from 80 to 1000 μm). The working medium was water and the research aimed to find the best range of minigap depth in terms of heat flux transferred and pressure drop. The authors conducted the experiment for the mass flux in the range of 390 to 900 kg/$m^2$s with the supplied heat flux density up to 700 kW/$m^2$. In addition to the thermal measurements, the flow was visualized with a fast shutter speed camera. Thanks to it, it was possible to observe two-phase flow structures that appear in the minigap during boiling. The authors found that the heat transfer coefficient increases with the decrease of the minigap depth and the intense dryout phenomena were observed in the depth range from 100 to 500 μm. For minigap depths of 700 μm and more, bubbly flow is the dominant flow structure for low heat fluxes, while slug and annular flow appear with increasing heat flux.

Alam et al. [6] experimentally tested two heat exchangers using different minigeometries, i.e. a minigap and 30 parallel minichannels. In both heat exchangers, water with a temperature at the inlet to the section of 86 °C was a working medium. Boiling was realized by supplying a heat flux of up to 850 kW/$m^2$. The working medium mass flux ranged from 400 to 1000 kg/$m^2$s. The research aimed to compare the heat transfer coefficients and pressure drops for the mentioned minigeometries. Also, the authors took a closer look at the hotspots, which are a consequence of the flow maldistribution phenomenon. The results showed that the minigap heat exchanger offers a very promising performance with high heat flux and low mass flux. Pressure drops are smaller in the minigap compared to a set of parallel minichannels. Unlike minichannels, the minigap allows bubbles to grow both in the flow direction and in the perpendicular direction of the flow, which minimizes pressure and temperature fluctuations in the heat exchanger.

Alam and Lee [26] conducted further experimental work investigating the flow of water in an expanding minigap under diabatic conditions. The authors tested three minigeometries of the same depth at the inlet (200 μm) but different depths at the outlet: 200 (conventional), 300, and 460 μm. As in previous works, the mass flux varied in the range of 400 to 1000 kg/$m^2$s, and the heat flux density did not exceed 800 kW/$m^2$. In the research, a fast shutter speed camera was used to visualize the boiling structures. The results of these studies show that the use of expanded minigaps results in better fluid distribution and thus a more uniform wall temperature field than for a conventional minigap (non-expanding). Moreover, the authors observed an intensified heat transfer and improved heat transfer coefficient on account of reduced flow boiling instabilities. This is due to the extra space for the bubbles to develop in the flow direction. Nevertheless, too much extension of the minigap results in the loss of the heat transfer intensification effect. The authors emphasized that further systematic researches into minigap heat exchangers are needed.

A new idea of combining both minigeometries, namely minigaps and minichannels in a single heat exchanger, was proposed by Mathew et al. [7]. The research was carried out for five different mass flow rates of water with a temperature of 85.5 °C in the range of 100 to 399 kg/$m^2$s. Innovative hybrid heat exchanger, which consisted of 40 parallel minichannels (12.5 mm long and a rectangular cross-section of 0.6 mm × 0.3 mm) and 12.5 mm long, 25 mm wide, and 0.6 mm deep minigap, showed good thermohydraulic properties. The proposed heat exchanger offered combined advantages of both designs i.e. excellent heat transfer coefficients, good stability during boiling, and lower pressure drop compared to the classic minichannel heat exchanger.

Klugmann et al. [27] compared the performance of a minigap heat exchanger (0.5 mm deep and 100 mm wide) to an equivalent minichannel heat exchanger (50 parallel rectangular minichannels of size 1 mm × 1 mm) in their two-phase flow experimental study on ethanol.

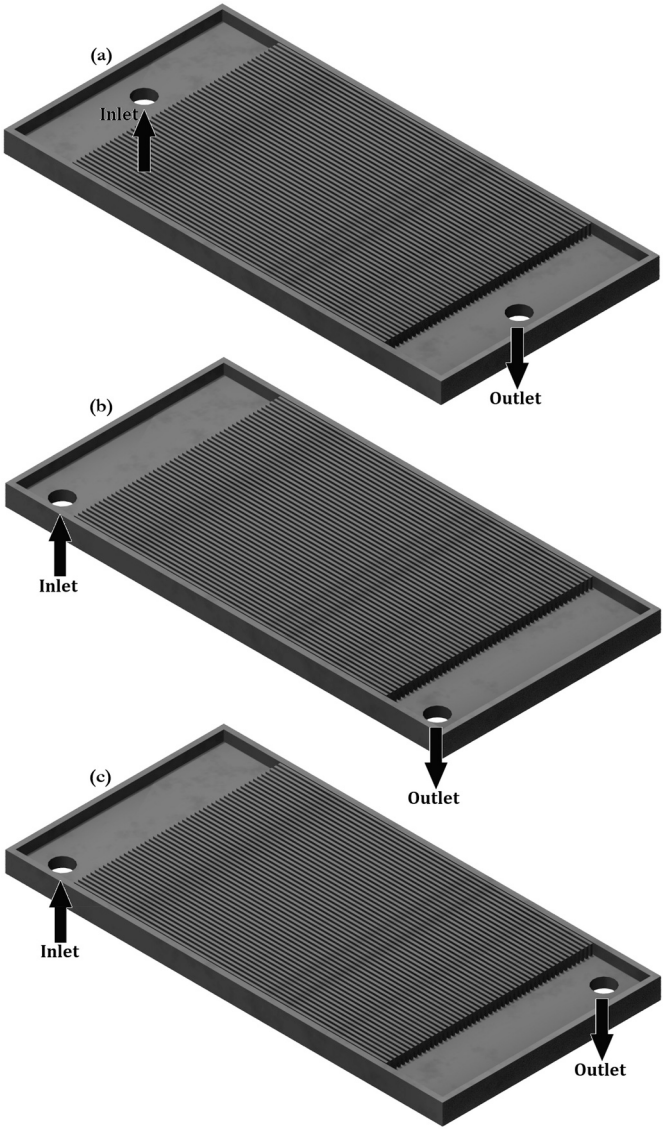


**Fig. 1.** Types of flow configurations in heat exchangers for perpendicular flow direction of manifolds: (a) I-type, (b) C-type, (c) V-type.

The authors have analyzed the efficiency of heat transport and pressure drop depending on the system operating parameters. The section cover was transparent to visualize the flow structures. The authors noticed differences between the minigap and minichannel sections in terms of local heat transfer coefficient distribution and visible differences in two-phase flow.

The above consideration follows that the studies on heat exchangers using minigeometries are carried out very intensively worldwide. Both minichannels and minigaps are characterized by high heat transfer coefficients and high compactness. However, both minigeometries are problematic in terms of nomenclature and in determining the specific value that defines the transition from minigap to minichannel. The flow boiling characteristics in both geometries are quite different. Minigaps enjoy the enriched benefits of minigeometry and at the same time suffer less problematic flow boiling instabilities associated with conventionally developed design (minichannels). Hence, defining the proper classification between minichannel and minigap is crucial. Moreover, the flow in minichannels and minigaps is different and some models validated during experiments on channels may not be valid in minigaps.

## 2. CFD model details

Before starting the numerical simulation, the minigeometries of various widths and depths with rectangular inlet and outlet manifolds have been designed. Three-dimensional models were created with the ANSYS SpaceClaim software and then the fluid domains were prepared. The working medium was assumed as ethanol. The fluid flows along the *Z*-axis.

### 2.1. Physical model

Flow configuration is essential for the study of heat exchangers or individual minichannels. There are many types of it in the literature, and unfortunately, different authors call a given type differently, and sometimes different configurations are hidden under the same name [28–32]. The configurations for the perpendicular inlet direction were selected that are the most common in the literature. They are shown in Fig. 1. It can be seen that the flow configuration depends on the relative position of the inlet and outlet, and their names are to suggest how the flow is implemented. In this paper, I-type and V-type flow configurations are analyzed.

The literature offers many design solutions for manifolds [28,33–41]. First of all, they differ in shape. The basic shapes that can be distinguished are shown in Fig. 2. These are exemplary, schematic manifolds that do not take into account the location of the fluid inlet but are only intended to symbolically represent the shape. For current simulations, rectangular manifolds have been chosen.

There were 18 different physical models of a section in V-type flow configuration and 18 with I-type flow configuration with various aspect ratios (α) and depths. The physical models of the section have been shown in Fig. 3 and all their specific dimensions were summarized in Table 2. In current studies, 18 physical models with a depth of 1 mm (9 in V-type and 9 in I-type) and 18 physical models with a depth of 0.5 mm (9 in V-type and 9 in I-type) have been tested. These sections differed in width so that their α was from 1 to 100. Thanks to that, it could be checked how the aspect ratio influences the flow of the working medium regardless of width and depth. The length of every minigeometry was 100 mm which is always greater than the entrance length [42,43] for every case. Minigeometry has always been in the symmetry axis of the manifolds.

### 2.2. Governing equations and boundary conditions

To investigate the effect of the aspect ratio of the minigeometry section on flow distribution and velocity profile following assumptions were taken:

- Properties of fluid were independent of pressure.
- Fluid flow was a single-phase, steady-state, incompressible, and three-dimensional.

The continuity and momentum equations (Eqs. (1) and (2)) were taken into account as governing equations and used in calculations together with the above-mentioned assumptions.

$$\nabla \cdot \vec{V} = 0 \tag{1}$$

$$\rho\left(\vec{V} \cdot \nabla \vec{V}\right) = -\nabla p + \mu \nabla^2 V \tag{2}$$

The gravity acceleration g = 9.81 m/s$^2$ is consistent with the direction of the Y-axis.

In ANSYS FLUENT 18.2 the conservation equations of mass and momentum are solved using the finite volume method (FVM). The momentum equation was discretized by the second-order upwind scheme. Model SST k-omega has been chosen as a turbulence model. As known, this model gives good results near a wall, which is desirable in

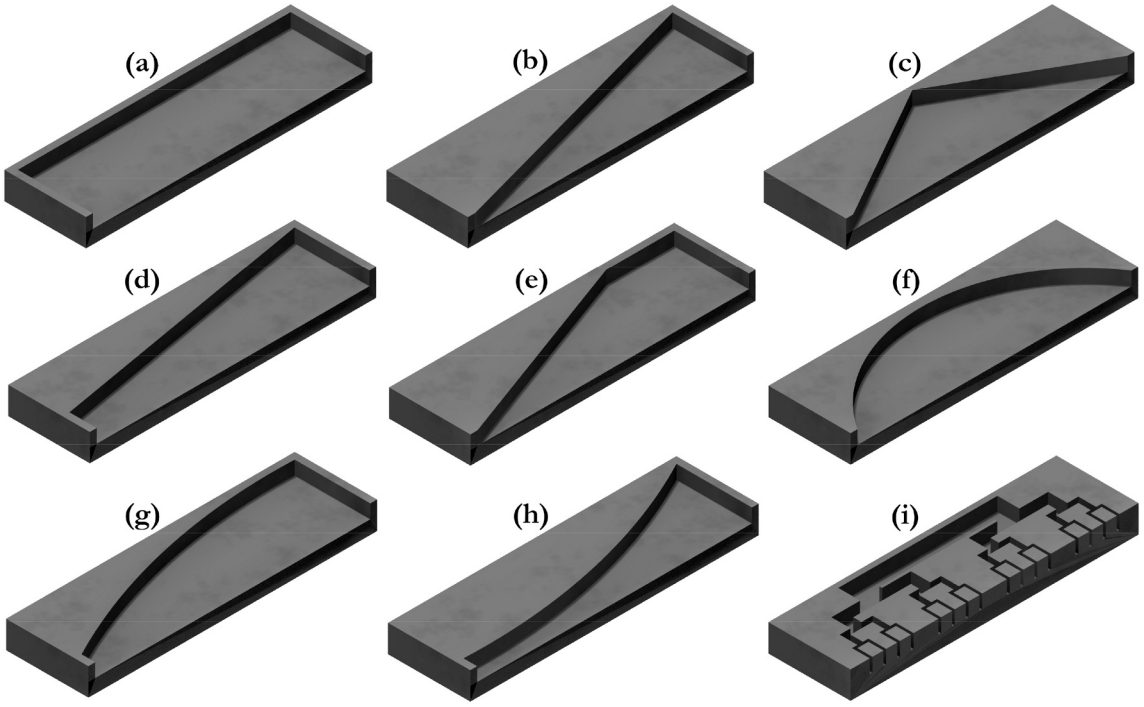


**Fig. 2.** The manifolds shape found in literature: (a) rectangular, (b) triangular I, (c) triangular II, (d) trapezoidal I, (e) trapezoidal II, (f) round, (g) convex, (h) concave, (i) bifurcation.

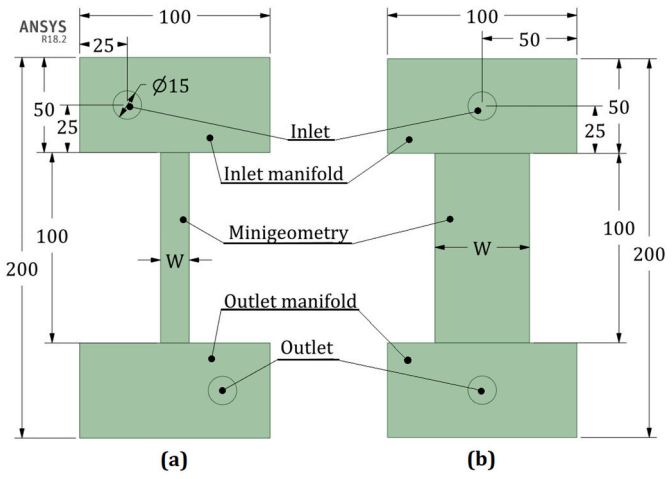


**Fig. 3.** The physical models of tested section (dimensions in mm) (a) V-type flow configuration, (b) I-type flow configuration.

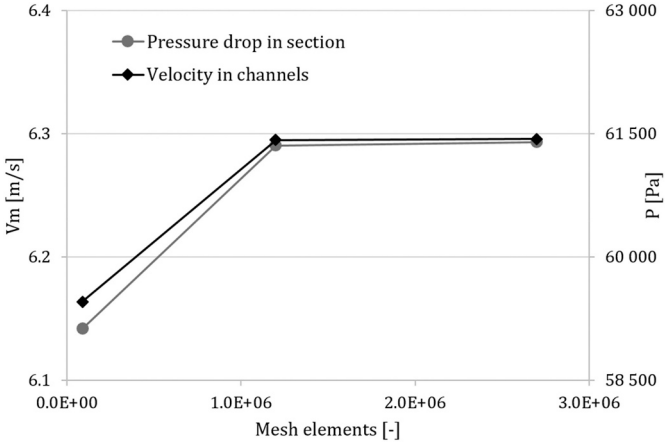


**Fig. 4.** The results of grid independence study.

**Table 2**
Dimensions of 18 cases tested during simulations.

| | d [mm] | | | |
|---|---|---|---|---|
| | 1.0 | | 0.5 | |
| α | W [mm] | $D_h$ [mm] | W [mm] | $D_h$ [mm] |
| 1 | 1 | 1.00 | 0.5 | 0.50 |
| 2 | 2 | 1.33 | 1.0 | 0.67 |
| 5 | 5 | 1.67 | 2.5 | 0.83 |
| 7 | 7 | 1.75 | 3.5 | 0.88 |
| 9 | 9 | 1.80 | 4.5 | 0.90 |
| 10 | 10 | 1.82 | 5.0 | 0.91 |
| 12 | 12 | 1.85 | 6.0 | 0.94 |
| 50 | 50 | 1.96 | 25.0 | 0.98 |
| 100 | 100 | 1.98 | 50.0 | 0.99 |

small α minigeometries, and good results in bigger volume, which is desirable in high α minigeometries. A segregated implicit solver with the Coupled pressure correction algorithm has been chosen to compute the velocity field in the whole section.

Ethanol was chosen as a working fluid for all the considered cases. The inlet parameters for ethanol are $\rho = 790.0$ kg/m$^3$ and $\mu = 1.2 \times 10^{-3}$ Pa s. The mass flow rate was selected to ensure a constant Reynolds number of 4167 for every aspect ratio. This value of Reynolds number has been chosen to ensure turbulent flow and makes entrance length [42,43] not higher than 100 mm for every case. This approach was implemented for each of 2 depths resulting in 36 cases tested during a numerical simulation (differed in width, depth, aspect ratio, hydraulic diameter, mass flow rate, and flow configuration). The mass flow rate varied from $2.5 \times 10^{-3}$ kg/s to $1.2625 \times 10^{-1}$ kg/s depends on the hydraulic diameter and aspect ratio of the minigeometry. The pressure-outlet boundary condition was assumed at the outlet of the tested section. When the residual values become less than $10^{-6}$ for the continuity,

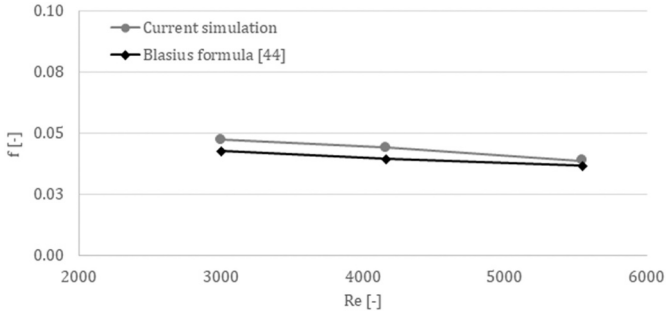


**Fig. 5.** The comparison of friction factor obtained during the simulation and friction factor calculated from Blasius formula [44].

x-velocity, y-velocity, and z-velocity, the solutions are considered to be converged.

## 3. Model validation

The fluid domain was discretized using ANSYS Fluent with tetrahedral control in a whole section. The mesh independence study was carried out to ensure the accuracy of numerical results. There were three different mesh types tested: Coarse ($9.0 \times 10^4$ elements), Medium ($1.2 \times 10^6$ elements), and Fine ($2.7 \times 10^6$ elements). The results of the V-type flow configuration minigeometry section with $\alpha = 1$ and $D_h = 1$ mm grid independence study were shown in Fig. 4. Results showed that the absolute percentage deviation between Medium and Fine mesh type is less than 1% for pressure drop and the average velocity in minigeometry as well. The Medium mesh has been chosen for further calculations.

A computational mesh that was used during all simulations consisted of from $7.7 \times 10^5$ to $13.1 \times 10^6$ elements depends on the width and depth of minigeometry.

To validate the model, a predicted friction factor from the simulation was compared with the well-accepted theoretical correlation of Blasius [44]. The results of the I-type flow configuration minigeometry section

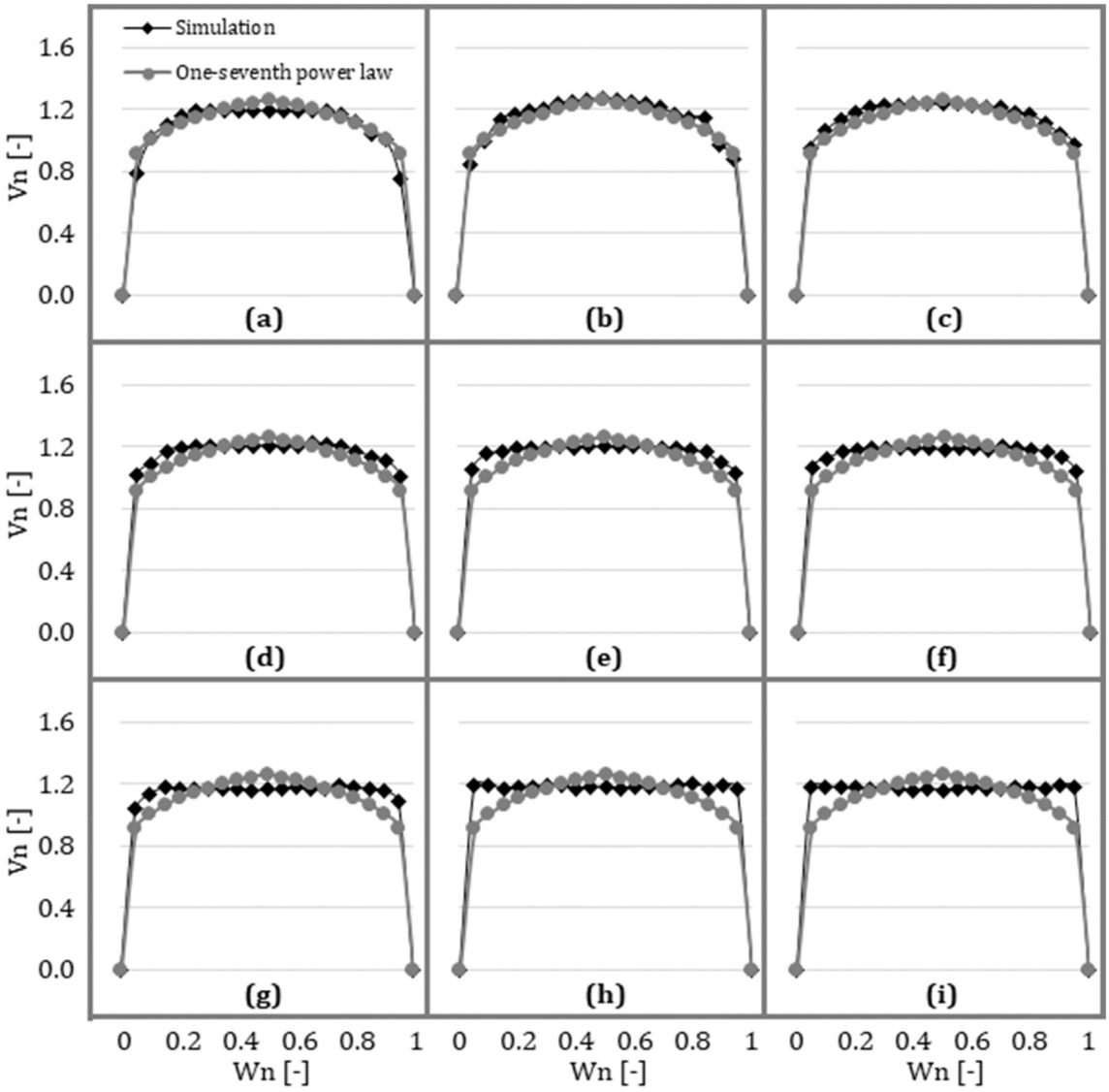


**Fig. 6.** The normalized velocity profile in I-type flow configuration over the normalized width for constant depth (d = 0.5 mm) and various aspect ratio (a) $\alpha = 1$, $D_h = 0.50$ mm, (b) $\alpha = 2$, $D_h = 0.67$ mm, (c) $\alpha = 5$, $D_h = 0.83$ mm, (d) $\alpha = 7$, $D_h = 0.88$ mm, (e) $\alpha = 9$, $D_h = 0.90$ mm, (f) $\alpha = 10$, $D_h = 0.91$ mm, (g) $\alpha = 12$, $D_h = 0.94$ mm, (h) $\alpha = 50$, $D_h = 0.98$ mm, (i) $\alpha = 100$, $D_h = 0.99$ mm.

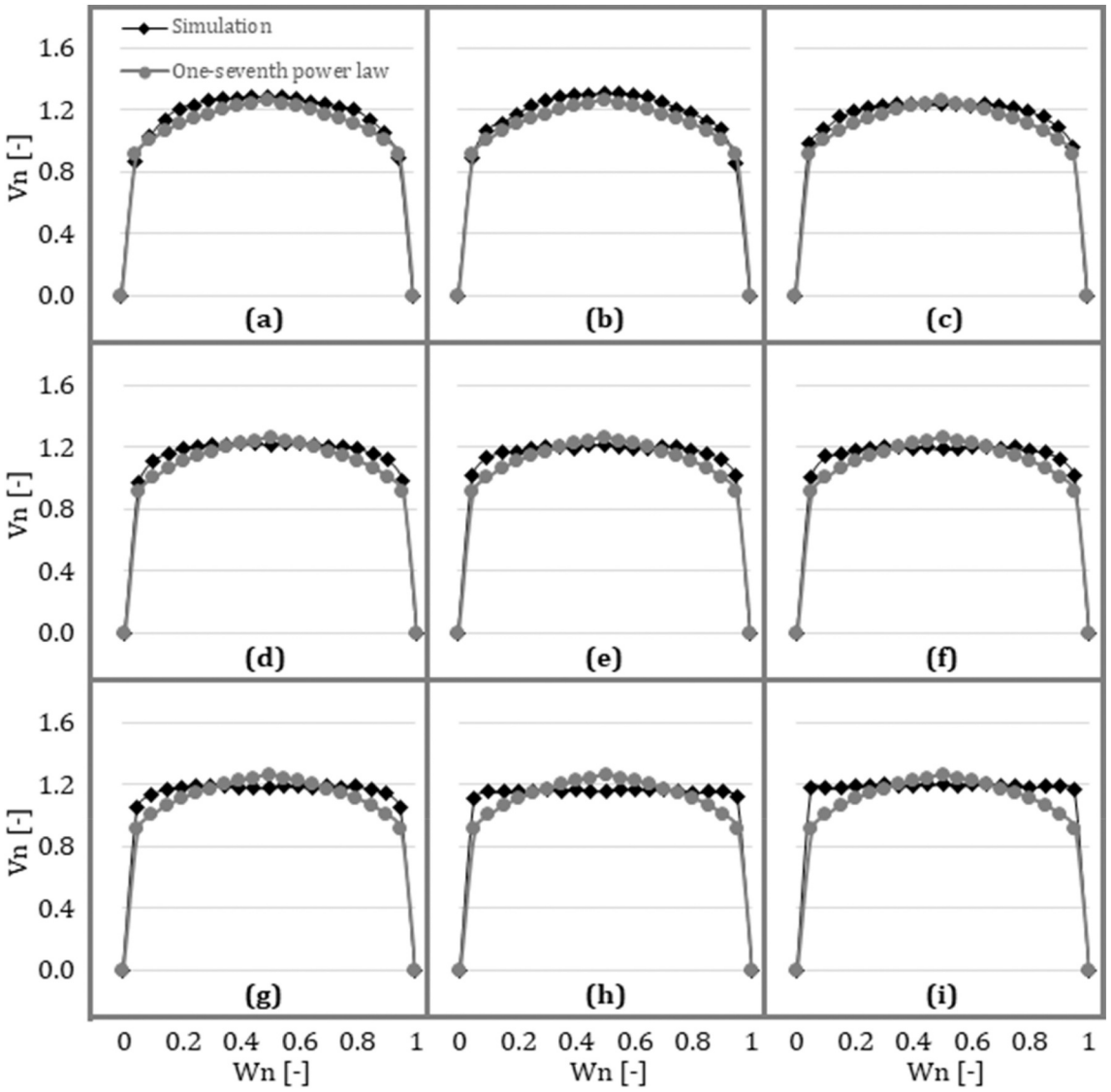


**Fig. 7.** The normalized velocity profile in I-type flow configuration over the normalized width for constant depth (d = 1.0 mm) and various aspect ratio (a) α = 1, $D_h$ = 1.00 mm, (b) α = 2, $D_h$ = 1.33 mm, (c) α = 5, $D_h$ = 1.67 mm, (d) α = 7, $D_h$ = 1.75 mm, (e) α = 9, $D_h$ = 1.80 mm, (f) α = 10, $D_h$ = 1.82 mm, (g) α = 12, $D_h$ = 1.85 mm, (h) α = 50, $D_h$ = 1.96 mm, (i) α = 100, $D_h$ = 1.98 mm.

with α = 2 and Dh = 1.33 mm were shown in Fig. 5. Results showed that the absolute percentage deviation between simulation and correlation friction factor is about 10%. A good agreement between the model and Blasius correlation ensures the accuracy and reliability of current numerical results.

## 4. Results and discussion

Since many minigeometries with different cross-section dimensions were checked, the geometric and flow parameters had to be normalized so that it was easy to compare different minigeometries with each other. Hence, the normalized velocity and normalized width have been introduced. The normalized velocity is the velocity calculated at a specific point divided by mean velocity in a whole minigeometry. The mathematical expressions of normalized velocity and mean velocity have been shown in Eq. (3) and Eq. (4), respectively.

$$V_{n,i} = V_i / V_m \tag{3}$$

$$V_m = \frac{\dot{m}}{\rho \cdot A} \tag{4}$$

Moreover, the normalized width, which shows in which part of the total width of the minigeometry the point under consideration is located has been defined by Eq. (5).

$$W_{n,i} = \frac{W - W_i}{W} \tag{5}$$

To compare the simulation results with the theory of turbulent flow, the friction factor calculation using the Blasius formula was proposed [44]. Eq. (6) is valid for $3.0 \times 10^3 \leq Re \leq 2.0 \times 10^5$, which is consistent with all the studied parameters. Moreover, the maximum normalized velocity was proposed (Eq. (7)) according to turbulent flow theory [45]. Lastly, the one-seventh power-law velocity profile [45] is rearranged to include the normalized variables. The transformed formula based on this law is shown in Eq. (8).

$$f = 0.316 Re^{-1/4} \tag{6}$$

$$V_{n,t,max} = \left(1 + 1.33\sqrt{f}\right) \tag{7}$$

$$V_{n,t,i} = V_{n,t,max}(1 - W_n)^{1/7} \tag{8}$$

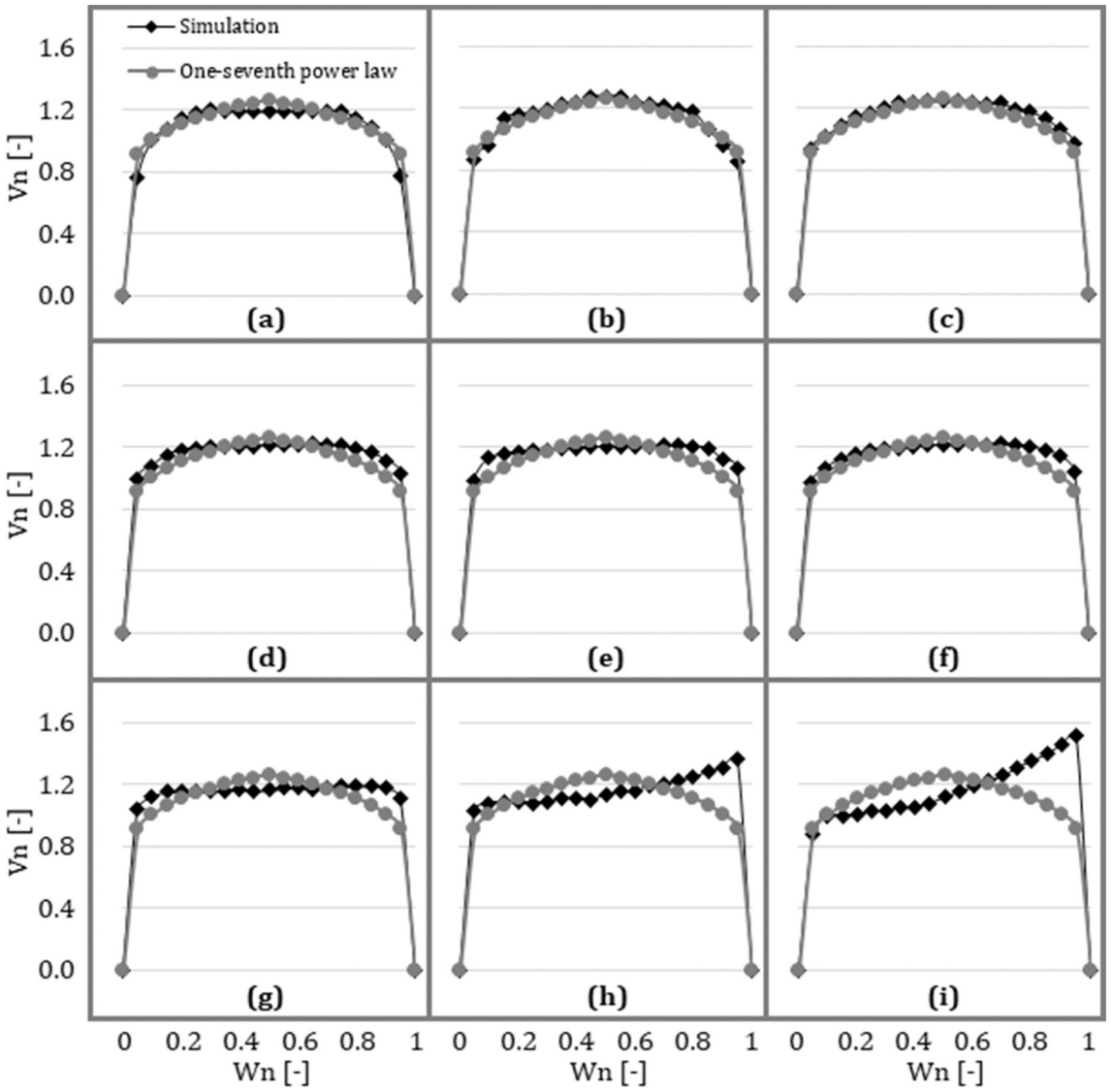


**Fig. 8.** The normalized velocity profile in V-type flow configuration over the normalized width for constant depth (d = 0.5 mm) and various aspect ratio (a) α = 1, $D_h$ = 0.50 mm, (b) α = 2, $D_h$ = 0.67 mm, (c) α = 5, $D_h$ = 0.83 mm, (d) α = 7, $D_h$ = 0.88 mm, (e) α = 9, $D_h$ = 0.90 mm, (f) α = 10, $D_h$ = 0.91 mm, (g) α = 12, $D_h$ = 0.94 mm, (h) α = 50, $D_h$ = 0.98 mm, (i) α = 100, $D_h$ = 0.99 mm.

The normalized velocity profiles over the normalized width for every case are analyzed. Each case's velocity profile is considered at a length greater than the entrance length to ensure stabilized flow without entrance phenomena. The geometries with a depth of 0.5 mm and I-type flow configuration have been compared in Fig. 6. It can be seen that the velocity profiles are changing with the increase of α. The case with α = 1 shows a typical velocity profile for turbulent flow. The fluid flow profile is symmetric of the central location and it does not differ much from the theoretical velocity distribution in a channel according to the one-seventh power-law (Eq. (8)). The above similarity between the simulated velocity profile and the theoretical velocity profile is maintained for α = 2 and α = 5. The case α = 7 starts being different, but still, the sufficient similarity remains with the power-law velocity profile. For higher aspect ratios, the profile near the walls deviates from theory more as α increases. The velocity profiles start looking flat. The situation is similar for minigeometries with a depth of 1.0 mm as shown in Fig. 7. The differences are negligible. The α = 7 still looks like a threshold for velocity profile behavior changing.

The normalized velocity profiles over the normalized width for geometries with the depth of 0.5 mm and 1.0 mm and V-type flow configuration are shown in Fig. 8 and Fig. 9, respectively. In this case, the velocity profile behaves similar to the case described above, up to α = 5 (despite different depths of minigeometries or mass flow rates). With the increase in α, the velocity profile starts being asymmetric with a tendency of localizing maximum velocity on the right side of the geometry (due to V-type flow arrangement). In I-type flow configuration cases, the velocity profiles in minigeometries with α higher than 7 started to be flat. Nevertheless, the changing behavior is visible regardless of the flow configuration.

The quantitative comparison of velocity distribution in minigeometry obtained through the simulation and that calculated from the power-law was realized by standard deviation analysis. The normalized velocity deviation was introduced and shown in Eq. (9). It shows how the velocity profile obtained from simulation differs from the theory-based velocity profile obtained from the power law.

$$\sigma = \sqrt{\frac{\sum_{i=1}^{n} \left(V_{n,s,i} - V_{n,t,i}\right)^2}{n}} \times 100\% \tag{9}$$

In Fig. 10, the normalized velocity deviation versus aspect ratio for various depths of minigeometries for I-type flow configuration has been

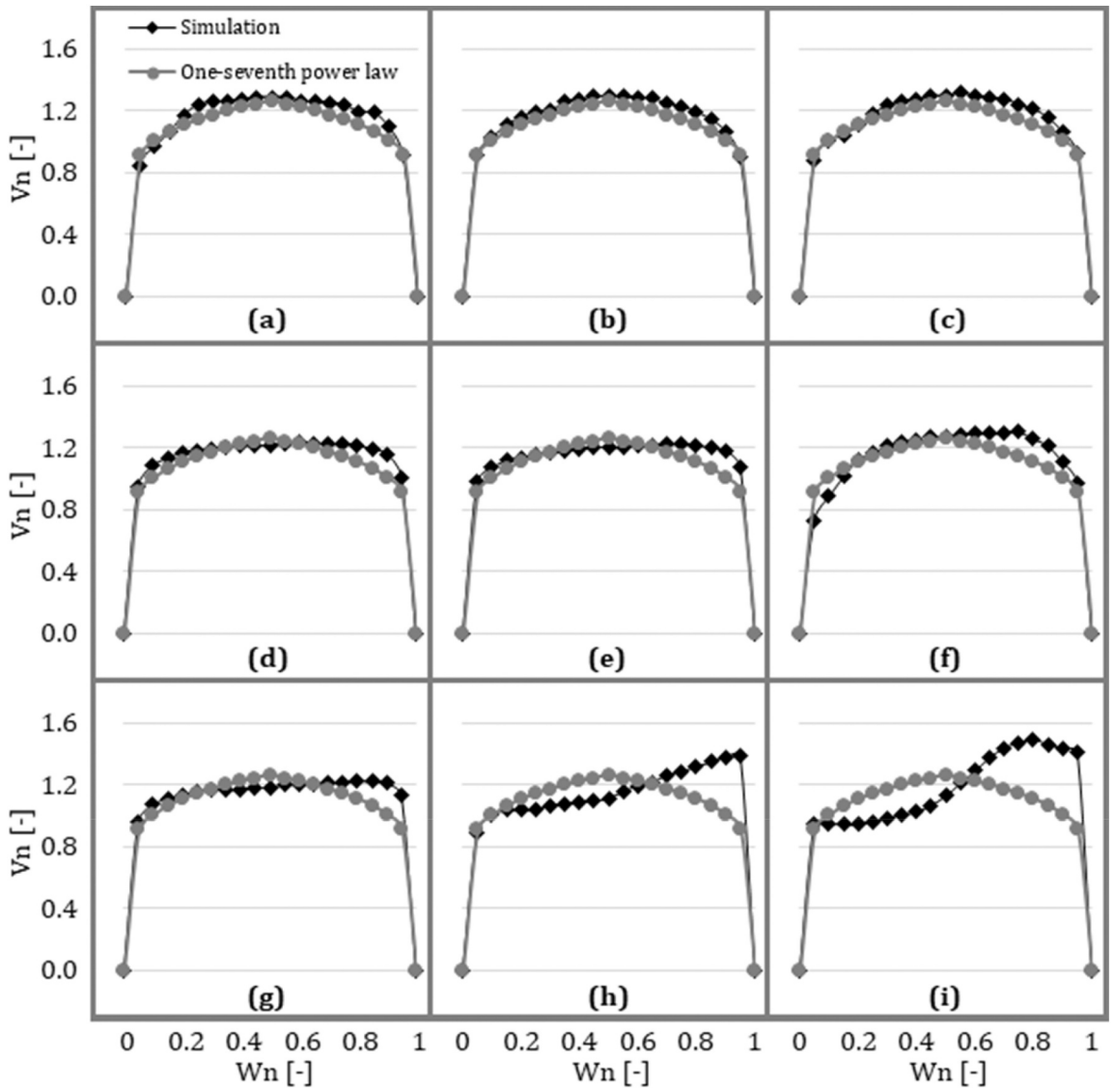


**Fig. 9.** The normalized velocity profile in V-type flow configuration over the normalized width for constant depth (d = 1.0 mm) and various aspect ratio (a) α = 1, $D_h$ = 1.00 mm, (b) α = 2, $D_h$ = 1.33 mm, (c) α = 5, $D_h$ = 1.67 mm, (d) α = 7, $D_h$ = 1.75 mm, (e) α = 9, $D_h$ = 1.80 mm, (f) α = 10, $D_h$ = 1.82 mm, (g) α = 12, $D_h$ = 1.85 mm, (h) α = 50, $D_h$ = 1.96 mm, (i) α = 100, $D_h$ = 1.98 mm.

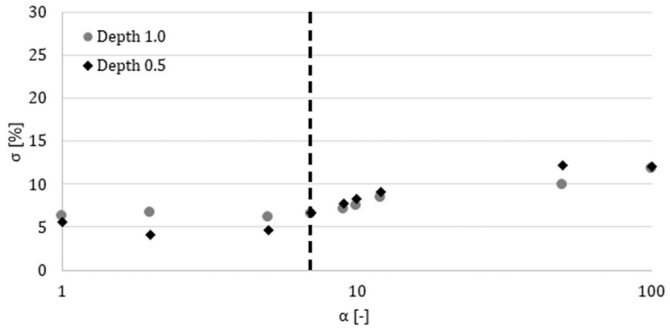


**Fig. 10.** The normalized velocity deviation for various aspect ratios and depth of minigeometry for I-type flow configuration (the abscissa axis is presented in a logarithmic scale).

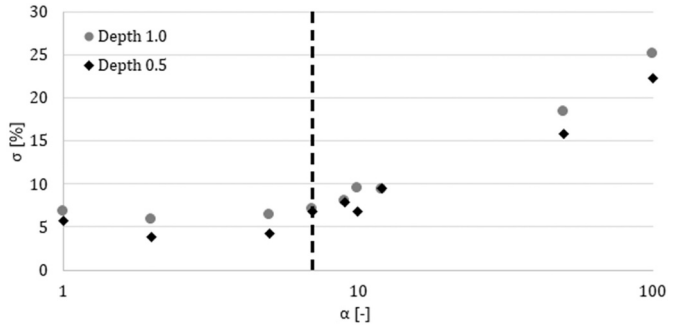


**Fig. 11.** The normalized velocity deviation for various aspect ratios and depth of minigeometry for V-type flow configuration (the abscissa axis is presented in a logarithmic scale).

shown. The conducted analysis shows that there is no big difference between results for cases with a depth of 0.5 mm and a depth of 1.0 mm. It can be deduced that the aspect ratio plays the most important role in the deviation of the normalized velocity profile, not the hydraulic diameter or depth of minigeometry. Worth noticing that the abscissa axis is presented on a logarithmic scale. The normalized velocity

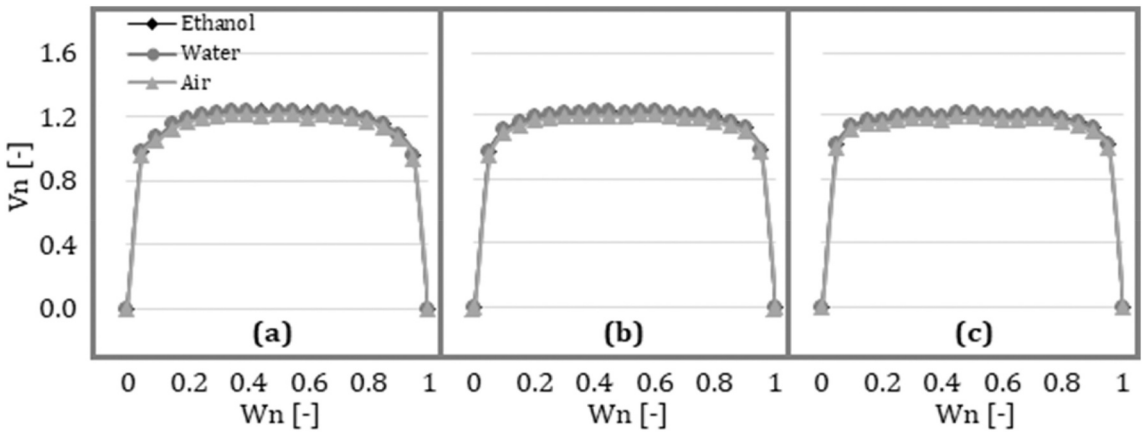


**Fig. 12.** The normalized velocity profile in I-type flow configuration over the normalized width for constant depth (d = 1.0 mm), various aspect ratio and various fluids (a) α = 5, $D_h$ = 1.67 mm, (b) α = 7, $D_h$ = 1.75 mm, (c) α = 9, $D_h$ = 1.80 mm.

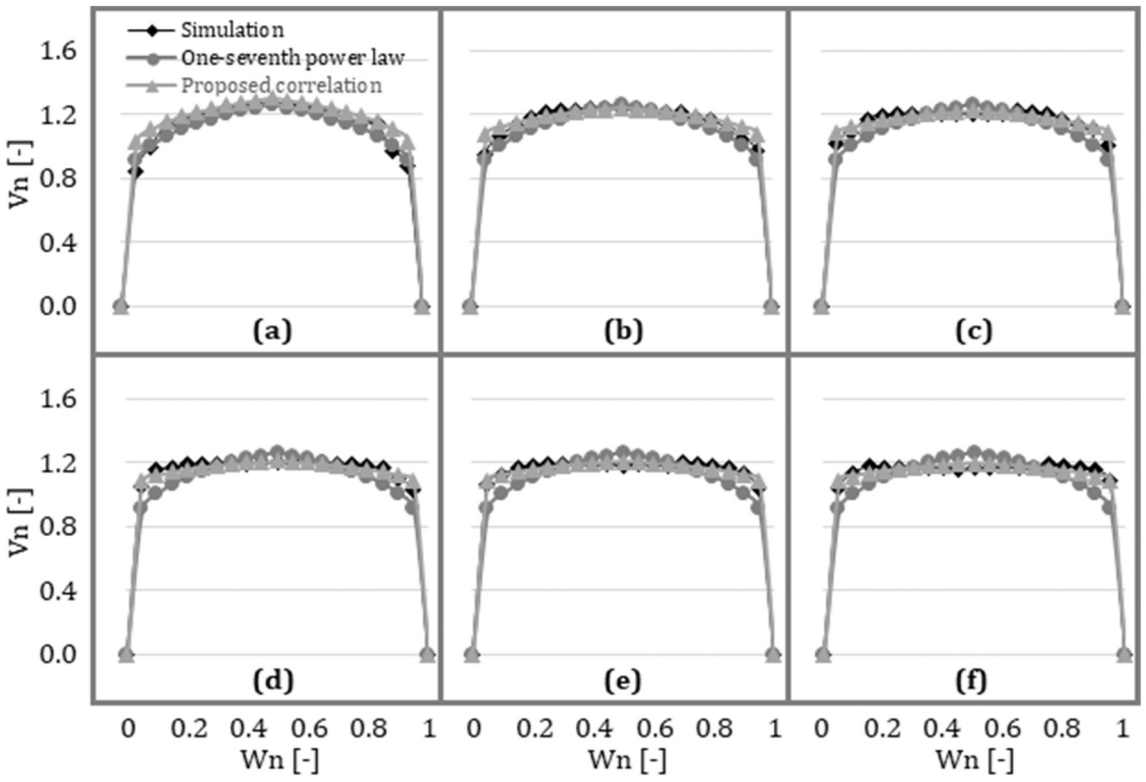


**Fig. 13.** The normalized velocity profile in I-type flow configuration over the normalized width for constant depth (d = 0.5 mm) and various aspect ratio (a) α = 2, $D_h$ = 0.67 mm, (b) α = 5, $D_h$ = 0.83 mm, (c) α = 7, $D_h$ = 0.88 mm, (d) α = 9, $D_h$ = 0.90 mm, (e) α = 10, $D_h$ = 0.91 mm, (f) α = 12, $D_h$ = 0.94 mm.

deviation is about 5% for all aspect ratios from 1 to 7 for both depths. After that, the mentioned parameter starts to grow rapidly. The nature of the function changes noticeably at α = 7, regardless of the depth. It seems that α = 7 is a threshold of minigeometries' velocity profile behavior.

The V-type flow configuration cases show similar dependencies as the above-mentioned, which can be seen in Fig. 11. The normalized velocity deviation is still about 5% for all cases of α from 1 to 7 (regardless of depth). The behavior change of the function starts still at the α = 7 and it is even more visible, especially at the highest α.

To validate if the conclusions are valid for other fluids, the calculations have been conducted for 2 additional fluids, namely water, and air. The simulation procedure, boundary conditions, and all the parameters were the same as previously, except the working medium. The results have been shown in Fig. 12. As can be seen, the normalized velocity profiles are identical for ethanol, water, and air as a working fluid. It suggests that all the conclusions drawn for ethanol may be developed for every fluid.

## 5. Proposed correlation

A modification for the existing one-seventh power law has been proposed to get a better fit between velocity profiles from simulation and theoretical calculations. Hence, a new correlation that takes into account the aspect ratio of the minigeometry has been proposed. To calculate maximum normalized velocity, a new coefficient K has been introduced into Eq. (7) known from the turbulent flow theory [45]. Consequently, a new equation for maximum standard velocity in the

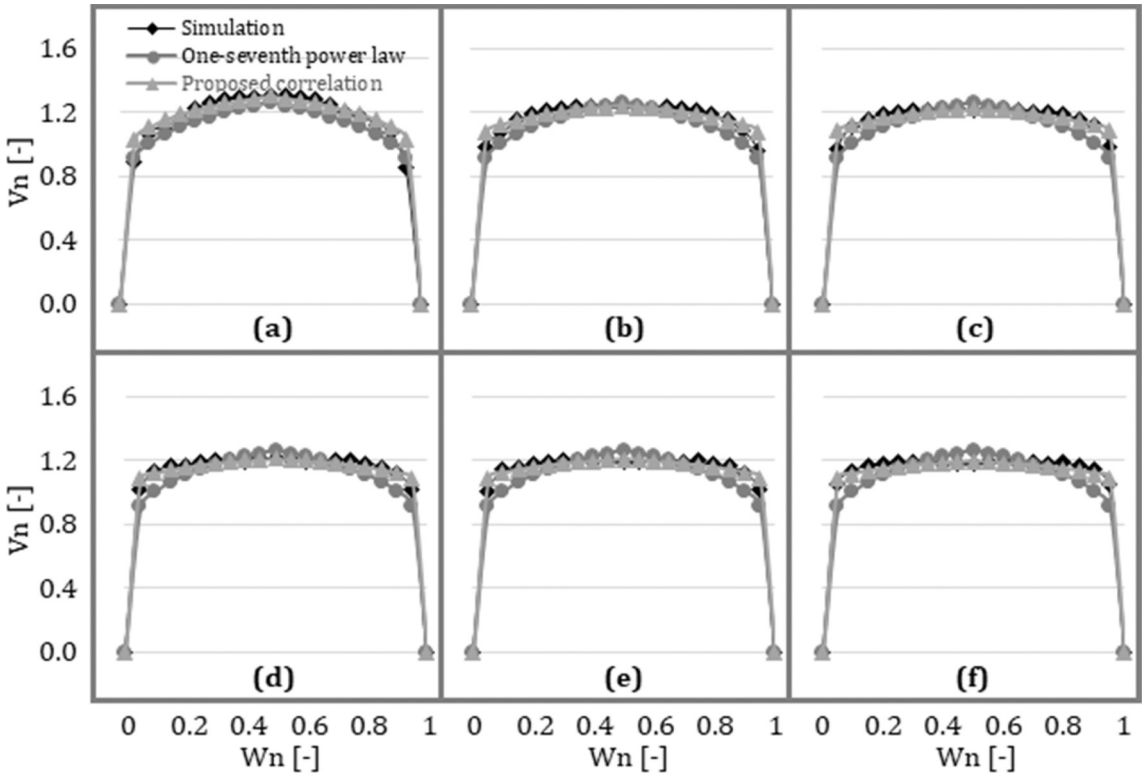


**Fig. 14.** The normalized velocity profile in I-type flow configuration over the normalized width for constant depth (d = 1.0 mm) and various aspect ratio (a) α = 2, $D_h$ = 1.33 mm, (b) α = 5, $D_h$ = 1.67 mm, (c) α = 7, $D_h$ = 1.75 mm, (d) α = 9, $D_h$ = 1.80 mm, (e) α = 10, $D_h$ = 1.82 mm, (f) α = 12, $D_h$ = 1.85 mm.

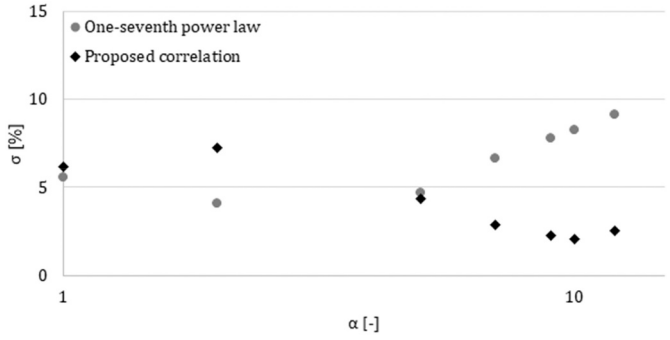


**Fig. 15.** The normalized velocity deviation (simulation vs theoretical calculation) for various aspect ratios of minigeometry for I-type flow configuration and d = 0.5 mm (the abscissa axis is presented in a logarithmic scale).

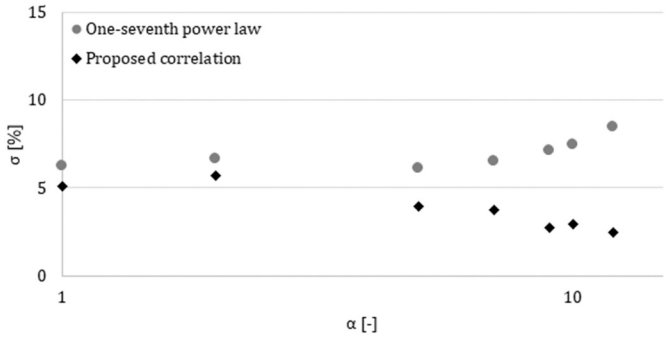


**Fig. 16.** The normalized velocity deviation (simulation vs theoretical calculation) for various aspect ratios of minigeometry for I-type flow configuration and d = 1.0 mm (the abscissa axis is presented in a logarithmic scale).

minigap is shown in Eq. (10). The mentioned coefficient K can be calculated from Eq. (11). The whole velocity distribution can be calculated from Eq. (12), where the aspect ratio has been incorporated. The described correlation for minigaps is valid for α = 7–12 and I-type flow configuration.

$$V_{n,t,max} = K\left(1 + 1.33\sqrt{f}\right) \tag{10}$$

$$K = -4.417 \times 10^{-6}\alpha^6 + 1.8667 \times 10^{-4}\alpha^5 - 3.1284 \times 10^{-3}\alpha^4 + 2.6241 \times 10^{-2}\alpha^3 - 1.1299 \times 10^{-1}\alpha^2 + 2.1625 \times 10^{-1}\alpha + 8.8623 \times 10^{-1} \tag{11}$$

$$V_{n,t,i} = V_{n,t,max}(1 - W_n)^{1/(7\sqrt{\alpha})} \tag{12}$$

The normalized velocity profiles obtained from simulation and calculated from one-seventh power law and proposed correlation can be seen in Fig. 13 and Fig. 14. It can be observed that a new correlation corresponds better than the one-seventh power law with the results for α ≥ 7 independently from depth. It flattens the velocity profile for higher aspect ratios.

The normalized velocity deviation versus aspect ratio for various depths of minigeometries for I-type flow configuration has been shown in Figs. 15 and 16. The calculations have been made between simulation results and one-seventh power law theoretical calculations and between simulation results and proposed correlation theoretical calculations.

It can be seen in Fig. 15 that for d = 0.5 mm cases the one-seventh power law gives better results than the proposed correlation for aspect ratios up to 5. For α = 7 or higher the opposite trend is visible. For d = 1.0 mm (Fig. 16) there is almost no difference between one-seventh power law and proposed correlation results for small aspect ratios. However, for higher aspect ratios a new correlation gives a lower standard deviation between simulated and theoretically calculated velocity profiles.

## 6. Conclusions

A detailed numerical investigation of 36 cases with constant Reynolds number and various aspect ratios, hydraulic diameter, and flow configuration was performed to investigate the effect of aspect ratio on the velocity profile. A 100 mm long α-varying minigeometries equipped with rectangular manifolds have been considered. The obtained normalized velocity profiles over the normalized width have been compared with the theoretical velocity distribution in a channel according to the one-seventh power law. Then the standard deviation analysis was introduced to show the difference between simulated and theoretically calculated velocity profiles. Based on the above results, the following conclusions were made.

The minigeometry depth does not influence significantly the fluid distribution but it can be seen that the velocity profiles are changing with the increase of α. The profiles are symmetric of the central location and it does not differ much from the theoretical velocity distribution up to $\alpha = 7$. The normalized velocity deviation grows rapidly after reaching that threshold. The flow in minigeometry with an aspect ratio greater than 7 should be treated two-dimensionally and the geometry itself be referred to as a minigap. Minichannel is the geometry with α up to 7.

The deviation between simulated and theoretically calculated velocity profiles is visible in the I-type flow configuration as well as in the V-type flow configuration. The rapid growth of the standard deviation can be seen for $\alpha = 7$ for both configurations. However, the V-type flow configuration shows a larger deviation in normalized velocity profiles, especially for high aspect ratios ($\alpha = 50$–100) due to a tendency of localizing maximum velocity on the right side of the geometry.

The proposed correlation for normalized velocity profile is valid for minigaps with $\alpha = 7$–12. The profiles obtained through the correlation correspond much better with the simulation results. There is still a need to validate the proposed correlation with some experimental data for various Reynolds numbers. It should also be developed for higher aspect ratios in future research.

## Declaration of Competing Interest

The authors declare that they have no known competing financial interests or personal relationships that could have appeared to influence the work reported in this paper.

## Acknowledgments

The work presented in this paper was funded from the National Science Centre, Poland research project No. 2017/27/N/ST8/02785 in the years 2018–2020.

## References

[1] J.F. Zhang, Y.K. Joshi, W.Q. Tao, Single phase laminar flow and heat transfer characteristics of microgaps with longitudinal vortex generator array, Int. J. Heat Mass Transf. 111 (2017) 484–494, https://doi.org/10.1016/j.ijheatmasstransfer.2017.03.036.
[2] Z. Wan, Y. Joshi, Pressure drop and heat transfer characteristics of pin fin enhanced microgaps in single phase microfluidic cooling, Int. J. Heat Mass Transf. 115 (2017) 115–126, https://doi.org/10.1016/j.ijheatmasstransfer.2017.06.117.
[3] C. Anbumeenakshi, M.R. Thansekhar, Experimental investigation of header shape and inlet configuration on flow maldistribution in microchannel, Exp. Thermal Fluid Sci. 75 (2016) 156–161, https://doi.org/10.1016/j.expthermflusci.2016.02.004.
[4] S. Kumar, P.K. Singh, Effects of flow inlet angle on flow maldistribution and thermal performance of water cooled mini-channel heat sink, Int. J. Therm. Sci. 138 (2019) 504–511, https://doi.org/10.1016/j.ijthermalsci.2019.01.014.
[5] J.Y. Song, S. Hah, D. Kim, S.M. Kim, Enhanced flow uniformity in parallel mini-channels with pin-finned inlet header, Appl. Therm. Eng. 152 (2019) 718–733, https://doi.org/10.1016/j.applthermaleng.2019.02.069.
[6] T. Alam, P.S. Lee, C.R. Yap, L. Jin, A comparative study of flow boiling heat transfer and pressure drop characteristics in microgap and microchannel heat sink and an evaluation of microgap heat sink for hotspot mitigation, Int. J. Heat Mass Transf. 58 (2013) 335–347, https://doi.org/10.1016/j.ijheatmasstransfer.2012.11.020.
[7] J. Mathew, P.S. Lee, T. Wu, C.R. Yap, Experimental study of flow boiling in a hybrid microchannel-microgap heat sink, Int. J. Heat Mass Transf. 135 (2019) 1167–1191, https://doi.org/10.1016/j.ijheatmasstransfer.2019.02.033.
[8] A.S. Dalkılıç, C. Özman, K. Sakamatapan, S. Wongwises, Experimental investigation on the flow boiling of R134a in a multi-microchannel heat sink, Int. Commun. Heat Mass Transf. 91 (2018) 125–137, https://doi.org/10.1016/j.icheatmasstransfer.2017.12.008.
[9] R. Ajith Krishnan, K.R. Balasubramanian, S. Suresh, The effect of heating area orientation on flow boiling performance in microchannels heat sink under subcooled condition, Int. J. Heat Mass Transf. 110 (2017) 276–293, https://doi.org/10.1016/j.ijheatmasstransfer.2017.03.030.
[10] J. Wajs, D. Mikielewicz, E. Fornalik-Wajs, Thermal performance of a prototype plate heat exchanger with minichannels under boiling conditions, J. Phys. Conf. Ser. 745 (2016), 032063, https://doi.org/10.1088/1742-6596/745/3/032063.
[11] E. Şimşek, S. Coskun, T. Okutucu-Özyurt, H.E. Unalan, Heat transfer enhancement by silver nanowire suspensions in microchannel heat sinks, Int. J. Therm. Sci. 123 (2018) 1–13, https://doi.org/10.1016/j.ijthermalsci.2017.08.021.
[12] T. Hempijid, C. Kittichaikarn, Effect of heat sink inlet and outlet flow direction on heat transfer performance, Appl. Therm. Eng. 164 (2019) 114375, https://doi.org/10.1016/j.applthermaleng.2019.114375.
[13] K. Strąk, M. Piasecka, B. Maciejewska, Spatial orientation as a factor in flow boiling heat transfer of cooling liquids in enhanced surface minichannels, Int. J. Heat Mass Transf. 117 (2018) 375–387, https://doi.org/10.1016/j.ijheatmasstransfer.2017.10.019.
[14] M. Piasecka, K. Strąk, B. Maciejewska, Calculations of flow boiling heat transfer in a Minichannel based on liquid crystal and infrared thermography data, Heat Transf. Eng. 38 (2017) 332–346, https://doi.org/10.1080/01457632.2016.1189272.
[15] A.B. Ozer, A.F. Oncel, D.K. Hollingsworth, L.C. Witte, A method of concurrent thermographic-photographic visualization of flow boiling in a minichannel, in: 2010 14th Int. Heat Transf. Conf. IHTC 14. 1, 2010, pp. 619–627, https://doi.org/10.1115/IHTC14-23107.
[16] B. Maciejewska, M. Piasecka, Time-dependent study of boiling heat transfer coefficient in a vertical minichannel, Int. J. Numer. Methods Heat Fluid Flow. (2019), https://doi.org/10.1108/HFF-12-2018-0781.
[17] M.H. Nasr, C.E. Green, P.A. Kottke, X. Zhang, T.E. Sarvey, Y.K. Joshi, M.S. Bakir, A. G. Fedorov, Flow regimes and convective heat transfer of refrigerant flow boiling in ultra-small clearance microgaps, Int. J. Heat Mass Transf. 108 (2017) 1702–1713, https://doi.org/10.1016/j.ijheatmasstransfer.2016.12.056.
[18] O.A. Kabov, D.V. Zaitsev, V.V. Cheverda, A. Bar-Cohen, Evaporation and flow dynamics of thin, shear-driven liquid films in microgap channels, Exp. Thermal Fluid Sci. 35 (2011) 825–831, https://doi.org/10.1016/j.expthermflusci.2010.08.001.
[19] F. Xu, H. Wu, Effect of pin-fins on the onset of flow instability of water in silicon-based microgap, Int. J. Therm. Sci. 130 (2018) 496–506, https://doi.org/10.1016/j.ijthermalsci.2018.05.020.
[20] M. Piasecka, Impact of selected parameters on refrigerant flow boiling heat transfer and pressure drop in minichannels, Int. J. Refrig. 56 (2015) 198–212, https://doi.org/10.1016/j.ijrefrig.2015.03.024.
[21] D. Lorenzini, C. Green, T.E. Sarvey, X. Zhang, Y. Hu, A.G. Fedorov, M.S. Bakir, Y. Joshi, Embedded single phase microfluidic thermal management for non-uniform heating and hotspots using microgaps with variable pin fin clustering, Int. J. Heat Mass Transf. 103 (2016) 1359–1370, https://doi.org/10.1016/j.ijheatmasstransfer.2016.08.040.
[22] P. Asrar, X. Zhang, C.E. Green, M. Bakir, Y.K. Joshi, Flow boiling of R245fa in a microgap with staggered circular cylindrical pin fins, Int. J. Heat Mass Transf. 121 (2018) 329–342, https://doi.org/10.1016/j.ijheatmasstransfer.2017.12.117.
[23] R. Ajith Krishnan, K.R. Balasubramanian, S. Suresh, Experimental investigation of the effect of heat sink orientation on subcooled flow boiling performance in a rectangular microgap channel, Int. J. Heat Mass Transf. 120 (2018) 1341–1357, https://doi.org/10.1016/j.ijheatmasstransfer.2017.12.133.
[24] A. Bar-Cohen, C. Holloway, A. Kaffel, A. Riaz, Waves and instabilities in high quality adiabatic flow in microgap channels, Int. J. Multiphase Flow 83 (2016) 62–76, https://doi.org/10.1016/j.ijmultiphaseflow.2016.03.016.
[25] T. Alam, P.S. Lee, C.R. Yap, L. Jin, K. Balasubramanian, Experimental investigation and flow visualization to determine the optimum dimension range of microgap heat sinks, Int. J. Heat Mass Transf. 55 (2012) 7623–7634, https://doi.org/10.1016/j.ijheatmasstransfer.2012.07.080.
[26] A. Tamanna, P.S. Lee, Flow boiling heat transfer and pressure drop characteristics in expanding silicon microgap heat sink, Int. J. Heat Mass Transf. 82 (2015) 1–15, https://doi.org/10.1016/j.ijheatmasstransfer.2014.11.047.
[27] M. Klugmann, P. Dąbrowski, D. Mikielewicz, Flow distribution and heat transfer in minigap and minichannel heat exchangers during flow boiling, Appl. Therm. Eng. 181 (2020), https://doi.org/10.1016/j.applthermaleng.2020.116034.
[28] G.D. Xia, J. Jiang, J. Wang, Y.L. Zhai, D.D. Ma, Effects of different geometric structures on fluid flow and heat transfer performance in microchannel heat sinks, Int. J. Heat Mass Transf. 80 (2015) 439–447, https://doi.org/10.1016/j.ijheatmasstransfer.2014.08.095.
[29] O.K. Siddiqui, S.M. Zubair, Efficient energy utilization through proper design of microchannel heat exchanger manifolds: a comprehensive review, Renew. Sust. Energ. Rev. 74 (2017) 969–1002, https://doi.org/10.1016/j.rser.2017.01.074.
[30] J. Cao, M. Kraut, R. Dittmeyer, L. Zhang, H. Xu, Numerical analysis on the effect of bifurcation angle and inlet velocity on the distribution uniformity performance of consecutive bifurcating fluid flow distributors, Int. Commun. Heat Mass Transf. 93 (2018) 60–65, https://doi.org/10.1016/j.icheatmasstransfer.2017.04.017.

[31] A.J. Mahvi, S. Garimella, Two-phase flow distribution of saturated refrigerants in microchannel heat exchanger headers, Int. J. Refrig. 104 (2019) 84–94, https://doi.org/10.1016/j.ijrefrig.2019.04.026.
[32] M. Saeed, M.H. Kim, Header design approaches for mini-channel heatsinks using analytical and numerical methods, Appl. Therm. Eng. 110 (2017) 1500–1510, https://doi.org/10.1016/j.applthermaleng.2016.09.069.
[33] J. Wang, H. Wang, Discrete method for design of flow distribution in manifolds, Appl. Therm. Eng. 89 (2015) 927–945, https://doi.org/10.1016/j.applthermaleng.2015.06.069.
[34] M.P. Vasilev, R.S. Abiev, R. Kumar, Effect of microchannel heat sink configuration on the thermal performance and pumping power, Int. J. Heat Mass Transf. 141 (2019) 845–854, https://doi.org/10.1016/j.ijheatmasstransfer.2019.07.031.
[35] R. Mandel, A. Shooshtari, M. Ohadi, Effect of manifold flow configuration on two-phase ultra-high flux cooling, Numer. Heat Transf. Part A Appl. 74 (2018) 1425–1442, https://doi.org/10.1080/10407782.2018.1538297.
[36] U. Madanan, D. Chatterjee, S.K. Das, A note on adiabatic two-phase flow maldistribution in a set of horizontal parallel minichannels with I-type and Z-type configurations, Chem. Eng. Process. Process Intensif. 132 (2018) 34–41, https://doi.org/10.1016/j.cep.2018.08.008.
[37] L.S. Maganti, P. Dhar, T. Sundararajan, S.K. Das, Heat spreader with parallel microchannel configurations employing nanofluids for near–active cooling of MEMS, Int. J. Heat Mass Transf. 111 (2017) 570–581, https://doi.org/10.1016/j.ijheatmasstransfer.2017.04.032.
[38] V. Manoj Siva, A. Pattamatta, S.K. Das, Effect of flow maldistribution on the thermal performance of parallel microchannel cooling systems, Int. J. Heat Mass Transf. 73 (2014) 424–428, https://doi.org/10.1016/j.ijheatmasstransfer.2014.02.017.
[39] I.A. Ghani, N.A. Che Sidik, N. Kamaruzzaman, W. Jazair Yahya, O. Mahian, The effect of manifold zone parameters on hydrothermal performance of micro-channel HeatSink: a review, Int. J. Heat Mass Transf. 109 (2017) 1143–1161, https://doi.org/10.1016/j.ijheatmasstransfer.2017.03.007.
[40] R. Kumar, G. Singh, D. Mikielewicz, A new approach for the mitigating of flow maldistribution in parallel microchannel heat sink, J. Heat Transf. 140 (2018) 72401–72410, https://doi.org/10.1115/1.4038830.
[41] P. Pluszka, A.P. Brenk, Z.M. Malecha, Numerical study of flow maldistribution in plate heat exchangers used for evaporation process, Arch. Thermodyn. 40 (2019) 57–82, https://doi.org/10.24425/ather.2019.129994.
[42] T.L. Bergman, F.P. Incropera, Fundamentals of Heat and Mass Transfer, Wiley, Hoboken, NJ, 2011.
[43] Y.A. Cengel, J.M. Cimbala, Fluid Mechanics : Fundamentals and Applications, McGraw-Hill Education, New York, NY, 2018.
[44] X. Fang, Y. Xu, Z. Zhou, New correlations of single-phase friction factor for turbulent pipe flow and evaluation of existing single-phase friction factor correlations, Nucl. Eng. Des. 241 (2011) 897–902, https://doi.org/10.1016/j.nucengdes.2010.12.019.
[45] S.B. Pope, Turbulent Flows, Cambridge University Press, 2000, https://doi.org/10.1017/CBO9780511840531.